METROLOGY AND MEASUREMENT SYSTEMS
Index 330930, ISSN 0860-8229
www.metrology.pg.gda.pl

DECISION SUPPORT SYSTEM FOR EPILEPTOGENIC ZONE LOCATION DURING BRAIN RESECTION

Marcin Kołodziej[1)], Andrzej Majkowski[1)], Remigiusz J. Rak[1)], Andrzej Rysz[2)], Andrzej Marchel[2)]

1) *Warsaw University of Technology, Institute of Theory of Electrical Engineering, Measurements and Information Systems, Koszykowa 75, 00-662 Warsaw, Poland* (✉ *marcin.kolodziej@ee.pw.edu.pl*, +48 22 234 7370, *andrzej.majkowski@ee.pw.edu.pl*, *remigiusz.rak@ee.pw.edu.pl*)
2) *Medical University of Warsaw, Department of Neurosurgery, Banacha 1A, 02-097 Warsaw, Poland* (*andrzej.rysz@wum.edu.pl*, *andrzej.marchel@wum.edu.pl*)

Abstract

This paper presents a system for locating the epileptogenic zone (EZ) using an automated analysis of electrocorticography (ECoG) signal recorded with 20 electrodes placed on the brain surface. The developed system enables automatic determination of places where anomalies connected with epilepsy are observed. The developed algorithm was tested on signals recorded for 33 patients who, after a prior neurological analysis, underwent the brain resection surgery. The results obtained with the algorithm were compared with those of medical analyses performed by the neurologist. The proposed system has a satisfactory accuracy – 87.8% – and can be used as a decision-supporting tool by the neurosurgeon during brain resection.

Keywords: ECoG, iEEG, electrocorticography, epileptogenic zone, signal analysis, expert system, neural network.

1. Introduction

Epilepsy is a disease that touches approximately 1–2% of the population [1]. Generally, the pathological synchronous activity of neurons starts at a small brain area localized within the grey matter and then spreads to its immediate vicinity, increasingly recruiting other parts of the brain (neurons). In the case of generalized epilepsy, the synchronous neural firing can affect the whole cortex, whereas, in the case of focal epilepsy only part of it is affected-a so-called epileptogenic zone (EZ) [2]. The major symptom of epilepsy is unexpected seizures, during which the patient loses control over his or her mind and body. This is dangerous to both the patient and the environment (especially if the patient is driving, passing the street etc.). Some patients use drugs that effectively reduce seizures. However, drugs do not help in 20–40% of the cases the seizures making normal functioning of the patients difficult.

The study on brain discharges related to epilepsy was launched in 1970, and it has since been a subject of intense research to date [8]. The widespread use of computer techniques had a significant impact on the attempt to detect these discharges. Very often, in the discussions

Article history: received on Jun. 10, 2017; accepted on Nov. 11, 2017; available online on Mar. 26, 2018, DOI: 10.24425/118167.

about epileptic discharges, reference is made to EEG signals, which of course are similar to electrocorticography (ECoG) signals. The analysis of EEG and ECoG signals, in the context of epilepsy, usually covers three separate issues: prediction of epileptic seizures, detection of the beginning of seizures, and identification of the channels in which the discharges occur [10, 11]. Numerous algorithms have been proposed for the detection of epilepsy based on the frequency analysis [12], time–frequency and wavelet analysis [13], artificial neural networks [14, 15], SVM classifiers [16], and data-mining tools [17]. The conventional time and frequency signal analysis was used in the works [18, 19, 20]. Much attention has been paid to the quantitative description and dynamics of signals [21, 22]. Also, the mutual correlation [23], Lapunov exponents [24, 25], and Kolmogorova entropy [26] were often used.

In some cases of epilepsy, it is possible to perform a complicated surgery–resection of that part of the brain where the source of epilepsy is localized. The key element that determines the success of the procedure is the exact location of the source of epilepsy, and then the complete removal of the relevant part of the brain [3]. In the preoperative phase, an EEG signal is used to locate the epileptic discharge area. It is often associated with forcing an epileptic seizure during the EEG registration and observation of the area in which discharges begin. Unfortunately, an EEG signal, due to the measurement method itself, is very noisy. The signal reaches the electrodes through the skull and the scalp. As a result, the location of an early onset of a seizure with the help of EEG is inaccurate. Hence, there is a need for a more accurate location of EZ. The precise location of EZ and determination of its boundaries give hope for a successful brain resection and improvement of the patient's condition. Resection of too small a part of the brain can cause further seizures; however, an unnecessary resection of too large an area of the brain can lead to significant dysfunctions.

To date, there has been a discussion on how to define EZ. ECoG is used to determine EZ accurately. In the case of ECoG (or intracranial electroencephalography – iEEG), the electrodes are placed directly on the exposed surface of the brain; thus, it is an invasive procedure. Using ECoG to determine EZ brings the following disadvantages [4]:

- Spontaneous epileptic activity consists exclusively of interictal spikes and sharp waves, and thus seizures are rarely recorded.
- It is impossible to distinguish the primary epileptic discharges from the secondary propagated discharges that arise at a distant epileptogenic site.
- Both background activity and epileptic discharges may be altered by anaesthetics, narcotic analgesics, and by the surgery itself.
- There is a limited duration of the surgery. Thus, if you are looking for a seizure activity during the intraoperative procedure, you may not see any.

One of the factors that significantly affect the correctness of the EZ location is a limited time that is at the neurosurgeon disposal during the operation. Using a 20-electrode grid, ECoG signals are recorded in a period of 8–15 min. In addition to the epilepsy-related discharges, morphologically similar discharges are also present in ECoG signals, which are a normal symptom of the brain activity. The analysis performed by the neurologist during a limited period of the open-brain surgery is stressful and does not enable to see all nuances in the ECoG signal. We attempted to develop a system for automated analysis of ECoG signals with the simultaneous indication of places in which epileptic discharges are initiated. The proposed algorithm enables analysing ECoG signals on the basis of their amplitude values and the frequency of occurrences of epilepsy discharges. EZ is shown in the graphical form on a plane covered by the electrode grid, with the help of which the neurologist can quickly confront the places he or she identified in the program result and can make an appropriate decision on the resection surgery.

2. Materials

ECoG signals acquired at the Medical University of Warsaw during the epilepsy surgery were analysed. Thirty-three patients who had drug-resistant focal epilepsy were examined: 13 males, 20 females (ages = 16–55, median = 35), with the duration of epilepsy between 6 and 45 years (median = 16 years). Twenty-seven patients suffered from lateral temporal epilepsy, and 6 patients – from medial temporal epilepsy [5, 6]. Temporal lobe pathologies were revealed in the cases with lateral temporal epilepsy: focal cortical dysplasia (FCD) type IIa (22 patients), type IIb (2 patients), type IIIb (2 patients), and cortical scar (1 patient), and in all remaining 6 cases of medial temporal epilepsy–hippocampal sclerosis [7]. An electrographic subdural grid of 20 electrodes (Fig. 1) was used for registration of pre-resection ECoG.

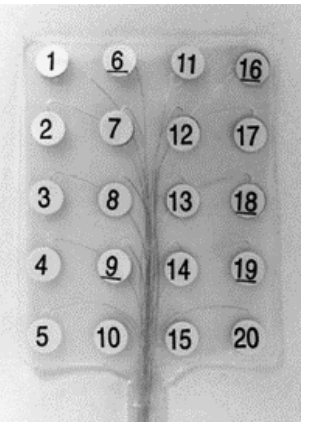

Fig. 1. An electrographic subdural grid of 20 electrodes used for ECoG registration.

ECoGs were recorded using a 0.5–70 Hz band-pass filtering and were 8–15 min long. A sample rate was 250 Hz.

3. Method

A functional scheme of the developed system for EZ determination is shown in Fig. 2. At first, an ECoG signal is subjected to low-band and band-pass filtration – "*Band-pass filtering*" and "*Low-pass filtering*." With these filters, the registered ECoG signal is divided into two independent parts of the following frequency ranges: signal 1 (0–3 Hz), signal 2 (12–22 Hz). Signal 1 is used to isolate epileptic discharges – spikes and poly-spikes, whereas signal 2 is used for extraction of artefacts. Both the signals are analysed in a similar way. A sliding time window termed "*Windowing*" and amplitude thresholds termed "*Thresholding*" are used to isolate components with a high energy content. "NOT" element placed in the artefact path performs the negation of binary matrix elements – the equivalent of the inversion of the signal phase. Then, the signal is passed through a "LOGICAL SECTION," the aim of which is to eliminate the data containing artefacts. After this, it is possible to count the spikes/poly-spikes by adding the binary matrix elements in rows – "*Calculation of the number of spikes*." In the last step spike amplitudes are evaluated – "*Calculation of spike amplitudes*."

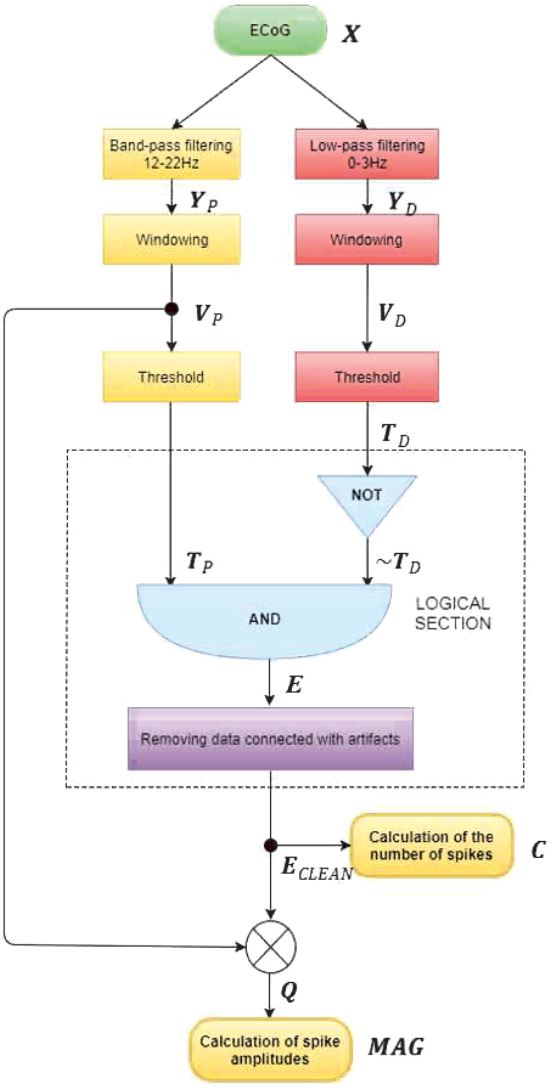

Fig. 2. A block diagram of our system for determining EZ.

ECoG signals were recorded using K channels, with N samples per channel. The formula $\boldsymbol{x}_k = [x_k(1)\ x_k(2)\ \ldots\ x_k(N)]$ denotes the k-th channel of the ECoG signal, containing N samples. A matrix $\boldsymbol{X}$ containing all the ECoG signals has the form:

$$\boldsymbol{X} = \begin{bmatrix} x_1(1) & x_1(2) & \ldots & x_1(N) \\ \vdots & \vdots & \vdots & \vdots \\ x_K(1) & x_K(2) & \ldots & x_K(N) \end{bmatrix} = \begin{bmatrix} \boldsymbol{x}_1 \\ \vdots \\ \boldsymbol{x}_K \end{bmatrix}. \tag{1}$$

The ECoG signals are subjected to a digital filtering process using infinite pulse-response (IIR) filters: "*Band-pass filtering*" and "*Low-pass filtering*." Filter coefficients b_k and a_k are se-

lected using the Butterworth filter design method. Vector samples after filtration are labelled as $\boldsymbol{y}_k = [y_k(1) \;\; y_k(2) \;\; \ldots \;\; y_k(N)]$. A current signal sample at the filter output is a linear combination of limited sets of input samples (size L) and output samples (size M), with corresponding weighting factors. It is described by a linear differential equation. For the first channel, it takes the form:

$$y_k(n) = \sum_{i=0}^{M} a_i y_k(n-i) + \sum_{i=0}^{L} b_i y_k(n-i). \tag{2}$$

As mentioned above (Fig. 2), we applied two types of filters: a band-pass filter $\boldsymbol{P}$ and a low-pass filter $\boldsymbol{D}$. After low-pass filtering, we obtained:

$$\boldsymbol{Y}_D = \begin{bmatrix} \boldsymbol{y}_{1D} \\ \vdots \\ \boldsymbol{y}_{KD} \end{bmatrix}; \tag{3}$$

and after band-pass filtering, we obtained:

$$\boldsymbol{Y}_P = \begin{bmatrix} \boldsymbol{y}_{1P} \\ \vdots \\ \boldsymbol{y}_{KP} \end{bmatrix}. \tag{4}$$

For each filtered signal, a sliding time window is used to extract its desired fragment "*Windowing*." For example, for channel k, a window with the starting point in the $n-$th sample and a width of$d$ samples can be chosen. As a result of this operation, we obtain vectors containing windowed signal samples after low-pass $\boldsymbol{w}_{kD}(n,d)$ and band-pass $\boldsymbol{w}_{kP}(n,d)$ filtering.

$$\boldsymbol{w}_{kD}(n,d) = [y_{kD}(n),\, y_{kD}(n+1),\, y_{kD}(n+2),\, \ldots,\, y_{kD}(n+d-1)]; \tag{5}$$
$$\boldsymbol{w}_{kP}(n,d) = [y_{kP}(n),\, y_{kP}(n+1),\, y_{kP}(n+2),\, \ldots,\, y_{kP}(n+d-1)]. \tag{6}$$

For each window of the $k-$th channel (after $\boldsymbol{D}$ and $\boldsymbol{P}$ filters), starting with the n-th sample and a width of d samples, it is possible to calculate the peak-to-peak (p–p) amplitude value of the signal:

$$V_{kD}(n) = \max\left(\boldsymbol{w}_{kD}(n,d)\right) - \min\left(\boldsymbol{w}_{kD}(n,d)\right); \tag{7}$$
$$V_{kP}(n) = \max\left(\boldsymbol{w}_{kP}(n,d)\right) - \min\left(\boldsymbol{w}_{kP}(n,d)\right). \tag{8}$$

From this operation, we obtain matrices $\boldsymbol{V}_D$ and $\boldsymbol{V}_P$ representing the p–p amplitudes associated with epilepsy and the ones associated with artefacts, respectively.

If a p–p amplitude in the window exceeds a certain threshold value, the value for this window is set to 1 (starting with the n-th sample) – "*Thresholding*":

$$t_{kD}(n) = \begin{cases} 0, & V_{kD}(n) < A_t \\ 1, & V_{kD}(n) \geq A_t \end{cases}, \tag{9}$$

where A_t is a threshold value for artefacts. Similarly,

$$t_{kP}(n) = \begin{cases} 0, & V_{kP}(n) < E_t \\ 1, & V_{kP}(n) \geq E_t \end{cases}, \tag{10}$$

where E_t is a threshold value for epilepsy discharges. As a result, we obtain vectors $\boldsymbol{t}_{kD}$ and $\boldsymbol{t}_{kP}$ in which the artefacts and spikes/poly-spikes are marked by 1 for channel k. Thus obtained matrices $\boldsymbol{T}_D$ and $\boldsymbol{T}_P$ represent the occurrences of epileptic artefacts and epileptic discharges, respectively.

$$\boldsymbol{T}_D = \begin{bmatrix} \boldsymbol{t}_{1D} \\ \vdots \\ \boldsymbol{t}_{KD} \end{bmatrix}; \tag{11}$$

$$\boldsymbol{T}_P = \begin{bmatrix} \boldsymbol{t}_{1P} \\ \vdots \\ \boldsymbol{t}_{KP} \end{bmatrix}. \tag{12}$$

To determine a binary matrix $\boldsymbol{E}$ that indicates epileptic discharges (without artefacts), the scalar product of matrix $\boldsymbol{T_P}$ and logically negated matrix $\boldsymbol{T}_D$ is calculated:

$$\boldsymbol{E} = \boldsymbol{T}_P \cdot (\sim \boldsymbol{T}_D), \tag{13}$$

where "~" is the logical negation operator – "NOT" and "$\cdot$" – the scalar product of matrices – "AND".
$E_{k,n}$ is an element of matrix $\boldsymbol{E}$ located in k-th row and n-th column.
$\boldsymbol{E}_k = [E_{k,1}\ E_{k,2}\ E_{k,3}\ \ldots\ E_{k,N}]$ depicts all elements of matrix $\boldsymbol{E}$ in a row k,
$\boldsymbol{E}_n = \begin{bmatrix} E_{1,n} \\ \vdots \\ E_{K,n} \end{bmatrix}$ depicts all elements of matrix $\boldsymbol{E}$ in a column n.

Unfortunately, as experience shows, such an analysis is not sufficient. It does not enable the removal of all artefacts. An example is an electrode movement artefact that appears in almost all channels. Therefore, additional methods were used to eliminate such artefacts as:

- artefacts at high frequencies that usually occur on all electrodes,
- artefacts of "floating electrodes", and
- high-frequency artefacts.

For this purpose, matrix $\boldsymbol{E}$ is modified by eliminating some rows and columns for which the sum of elements marked "1" exceeds the values of thresholds P_k or P_n – "*Removing data connected with artefacts*". We assume that such rows/columns contain artefacts.

Modification of all rows can be described by the formula:

$$\boldsymbol{E}_k = \begin{cases} \boldsymbol{0}, & \sum_{n=1}^{N} E_{k,n} \geq P_k N \\ \boldsymbol{E}_k, & \sum_{n=1}^{N} E_{k,n} < P_k N \end{cases}. \tag{14}$$

Modification of all columns can be described by the formula:

$$\boldsymbol{E}_n = \begin{cases} \boldsymbol{0}, & \sum_{k=1}^{K} E_{k,n} \geq P_n K \\ \boldsymbol{E}_n, & \sum_{k=1}^{K} E_{k,n} < P_n K \end{cases}. \tag{15}$$

As a result of these operations, we obtain a modified $\boldsymbol{E}$ matrix labelled $\boldsymbol{E}_{CLEAN}$, which should include only elements associated with the discharges associated with epilepsy.

Analysis of the $\boldsymbol{E}_{CLEAN}$ matrix enables to create a map of the epilepsy activity on each ECoG electrode. For electrode k, $k = 1,...,K$, the number of discharges associated with epilepsy is calculated by "*Calculation of the number of spikes*":

$$C_k = \sum_{n=1}^{N} E_{CLEAN_{k,n}} . \tag{16}$$

The result is a vector $\boldsymbol{C}$:

$$\boldsymbol{C} = \begin{bmatrix} C_1 \\ C_2 \\ C_3 \\ \vdots \\ C_K \end{bmatrix} . \tag{17}$$

This vector represents the frequency of occurrences of epilepsy discharges for each electrode. The values of vector $\boldsymbol{C}$ enable to indicate the electrodes with an increased activity of epileptic discharges.

It is also interesting to indicate amplitudes of discharges associated with epilepsy. To do this, we should calculate the scalar product of matrix $\boldsymbol{E}_{CLEAN}$, containing the discharge indicators associated with epilepsy, and matrix $\boldsymbol{V}_P$ containing the amplitudes of the discharges – "*Calculation of spikes amplitudes*":

$$\boldsymbol{Q} = \boldsymbol{E}_{CLEAN} \cdot \boldsymbol{V}_P . \tag{18}$$

For each electrode k, $k = 1...K$, we can calculate a value corresponding to the mean amplitude of epilepsy discharge:

$$MAG_k = \sum_{n=1}^{N} Q_{k,n} . \tag{19}$$

As a result, we obtain a vector $\boldsymbol{MAG}$:

$$\boldsymbol{MAG} = \begin{bmatrix} MAG_1 \\ MAG_2 \\ MAG_3 \\ \dots \\ MAG_K \end{bmatrix} . \tag{20}$$

A suitable illustration of elements of vector MAG (in the locations associated with individual electrodes) enables to indicate the electrodes on which the largest discharge amplitudes were recorded.

The proposed algorithm has some key input parameters:

d – a width of the analysis window expressed as the number of samples,

A_t – a threshold for artefacts,

E_t – threshold for epilepsy discharges,

P_k – a threshold for row elimination, and

P_n – a threshold for column elimination.

Apart from the aforementioned parameters, selecting parameters of the low-pass filters $\boldsymbol{D}$ and the band-pass filters $\boldsymbol{P}$ is also very important.

4. Results

The usefulness of the results generated by the algorithm was rigorously evaluated by the neurologist specializing in manual EZ determination. Thirty-three cases of ECoG recordings were analysed. The neurologist received activity maps generated by the program and confronted them with the ECoG signals, and declared either compliance or incompatibility of these results (algorithm vs. expert). During the assessment, he also noted the number of discharges and their amplitudes. As a result, the numbers of cases correctly diagnosed, incorrectly diagnosed and controversial ones were calculated. The results are summarized in Table 1. The condition of the correct diagnosis (Correctly recognized) was to properly identify the EZ regions. If one or more discrepancies were detected on any ECoG electrode, the system did not respond correctly (Incorrectly recognized). During testing, there was also one case where the neurologist was not entirely sure whether the detected discharges were associated with the EZ (Controversial).

Table 1. Effectiveness of the system compared with the results of the neurologist's analyses.

	Overall	**Correctly recognized**	**Incorrectly recognized**	**Controversial**
Number of cases	33	29	3	1
Percentage of cases	100%	87.87%	9.09%	3.03%

The graphical user interface (GUI) of the created program is shown in Fig. 3. It consists of 5 windows. Three windows on the left show from the top: recognized artefacts, recognized discharges, and the final result–epileptic discharges after removing artefacts. The window at the right top corner contains options for changing any possible algorithm settings. The window at the bottom right corner shows the analysed signal fragment. The program enables to read ECoG signals stored in the open EDF file format. This format is accepted by many utility programs for

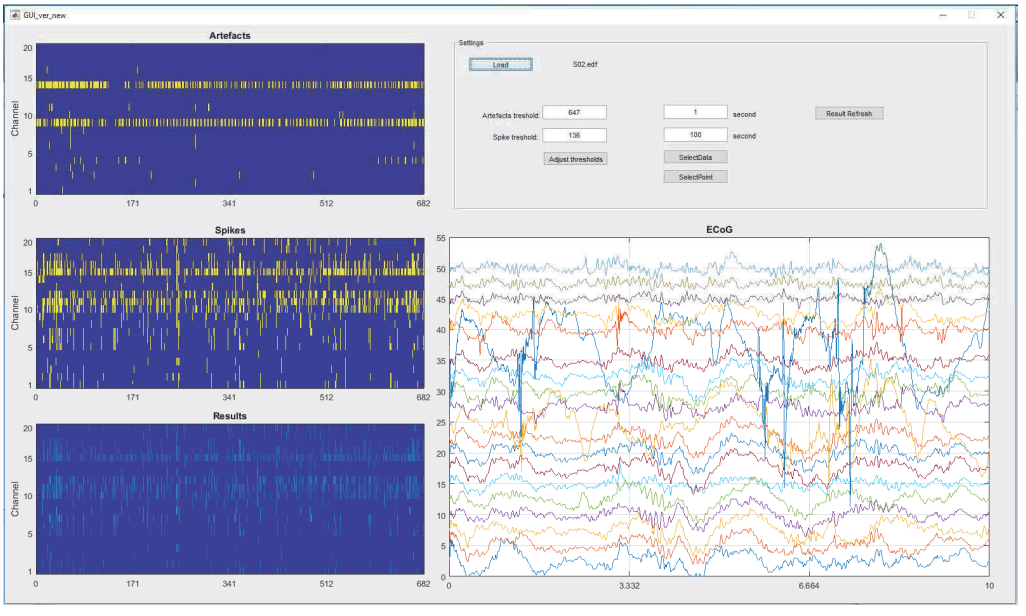

Fig. 3. The main panel of the created system for determining EZ.

recording biomedical signals. ECoG signals were recorded and analyzed using a special software developed by Elmiko at the Warsaw Medical University. The developed application enables, after loading the ECoG signals, the manual selection of a fragment to be analysed. This enables pre-elimination of the fragments with evident artefacts. Subsequently, the ECoG signal is filtered and threshold values for both spikes/poly-spikes and artefacts are selected. As a result of this action, for the entire marked ECoG signal, preliminary results are displayed showing:

– the occurrence of artefacts (Fig. 4a),
– the occurrence of spikes and the poly-spikes (Fig. 4b), and
– the amplitude of discharges of spikes and the poly-spikes (Fig. 4c).

In Fig. 4, the x-axis is scaled in seconds, and individual ECoG channels are arranged along the y-axis.

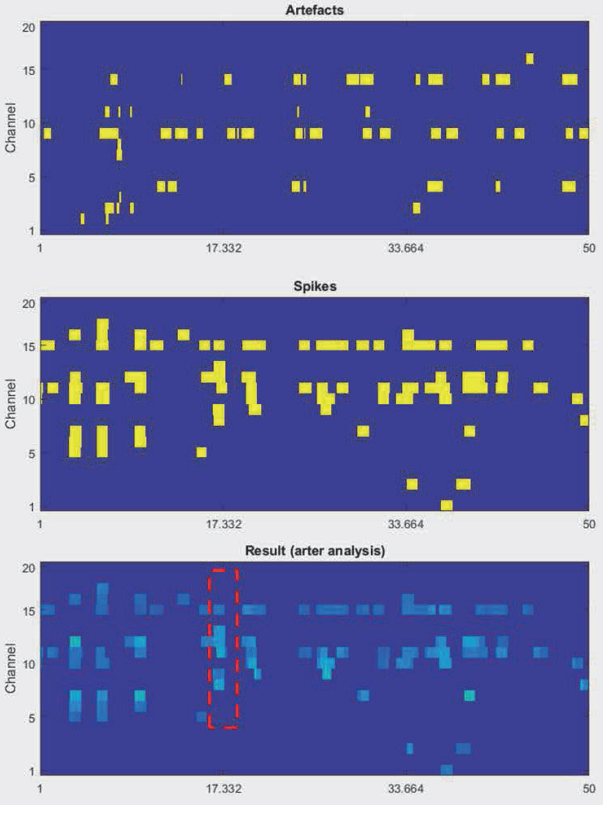

Fig. 4. a) Places of occurring artefacts; b) Places of occurring spikes and poly-spikes; c) An illustration of discharges (spikes and poly-spikes).

It is possible to mark the area of occurrence of discharges (Fig. 4c) and to view the corresponding ECoG signals (Fig. 5).

A proper selection of spikes' and artefacts' detection thresholds has a significant impact on the obtained results of removal of artefacts and detection of spikes/poly-spikes. These thresholds are selected automatically, using a multilayer perceptron (MLP) neural network. It is also possible to verify and possibly change the thresholds manually. After changing them, graphs showing the locations of artefacts and spikes/poly-spikes are updated automatically.

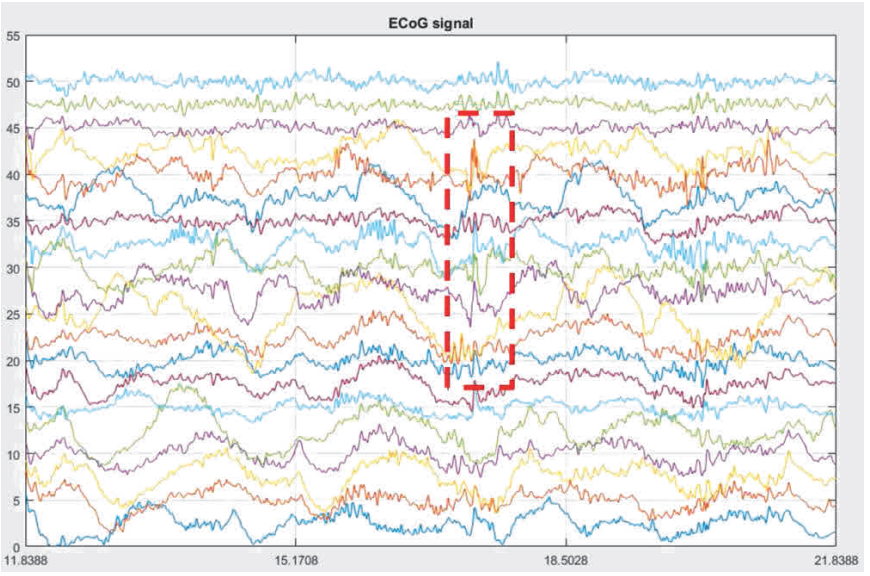

Fig. 5. An ECoG signal with a selected fragment.

The most important task of the developed system is to determine the areas with the highest activity of spikes/poly-spikes. Therefore, a module is provided in the algorithm that automatically generates activity maps showing:

– the frequency of occurrences of spikes/poly-spikes (Fig. 6), and
– the average amplitudes of spikes/poly-spikes determined for the whole analysed ECoG signal (Fig. 7).

The brighter the colour, the more frequent the spikes/poly-spikes or the greater their amplitudes. In Figs. 6 and 7, on the right, the interpolated results are displayed. Taking into account the

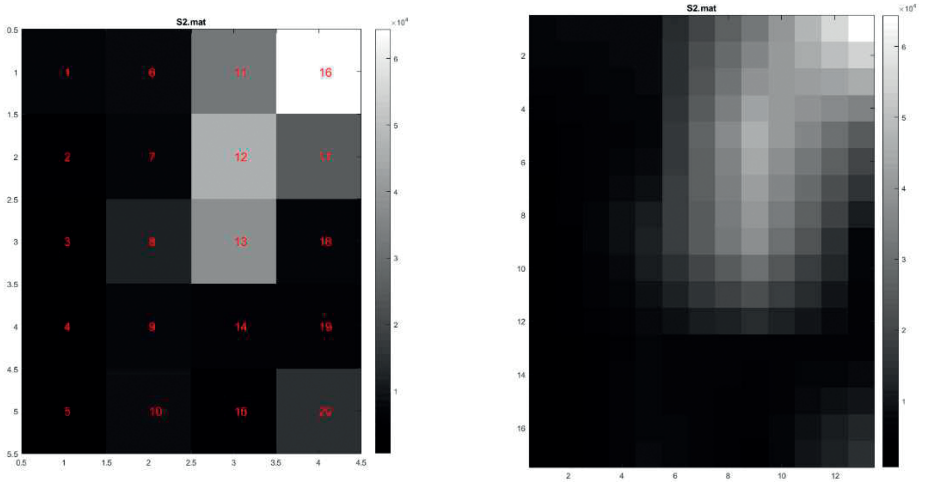

Fig. 6. Activity maps for spikes/poly-spikes.

placement of the electrode grid on the patient's brain, the neurosurgeon can quickly locate EZ and indicate the area subjected to the resection.

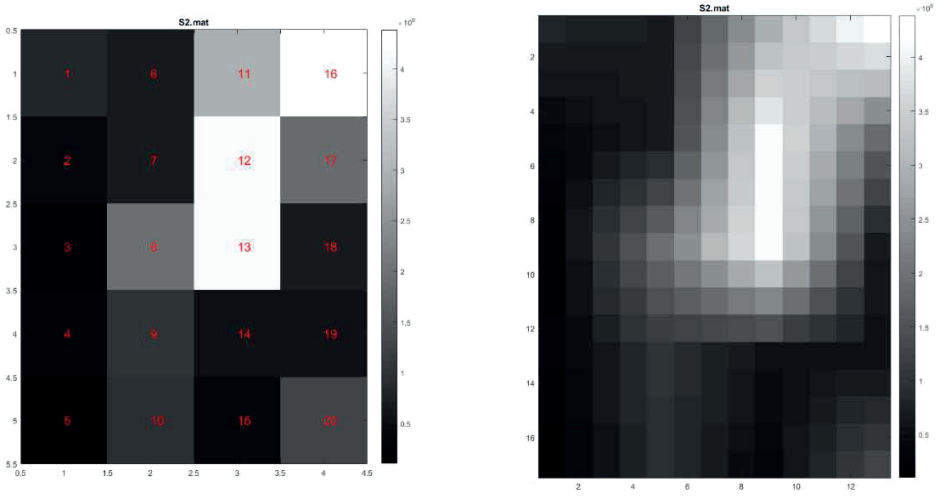

Fig. 7. Average amplitudes of spikes/poly-spikes determined for the analysed ECoG signals.

5. Discussion

In order to describe how the algorithm works, an analysis for one channel is presented. Figure 8 shows all intermediate signals used in the calculations: the registered ECoG signals, the detected spikes/poly-spikes and artefacts, and the final result, showing the occurrences of spikes/poly-spikes and their amplitudes.

Figure 8a shows the original ECoG signal for the k-th channel $(\boldsymbol{x}_k)$. Figure 8b (in red) shows the signal $(\boldsymbol{y}_{kP})$ after applying the band-pass filter (12–20 Hz). On the premises, the signal after such a filtration can be used to detect spikes/poly-spikes. Figure 8b (in blue) shows the amplitudes of spikes and poly-spikes $(\boldsymbol{V}_{kP})$. The dashed line indicates the detection threshold (E_t). The values that exceed the detection threshold are marked in magenta $(\boldsymbol{t}_{kP})$. These values indicate possible spikes/poly-spikes.

Figure 8c shows the ECoG signal (in red) $(\boldsymbol{y}_{kD})$ after the low-pass filtering (0–3 Hz). The signal after such a filtration can be used to detect low-frequency artefacts. The blue solid line indicates the amplitudes of the signal associated with the occurrences of artefacts $(\boldsymbol{V}_{kD})$. The fixed detection threshold for artefacts (A_t) is marked by the blue dashed line. The values that exceed the detection threshold are marked in purple $(\boldsymbol{t}_{kD})$. These are possible low-frequency artefacts.

In Fig. 8d, the partial detection of amplitudes of spikes and poly-spikes $(\boldsymbol{V}_{kD})$ is marked with blue. The signal fragments in which spikes occurred, and there were no artefacts $(\boldsymbol{E}_k)$ are indicated also with blue. We can also see the average time of spikes and poly-spikes (as the number of samples for which spikes/poly-spikes occurred) and the average amplitude of spikes and poly-spikes. In this way, for each channel k, $k = 1, \ldots K$, we are able to determine the image showing the time of occurrence of discharges in the form of spikes and poly-spikes of a sufficiently large amplitude.

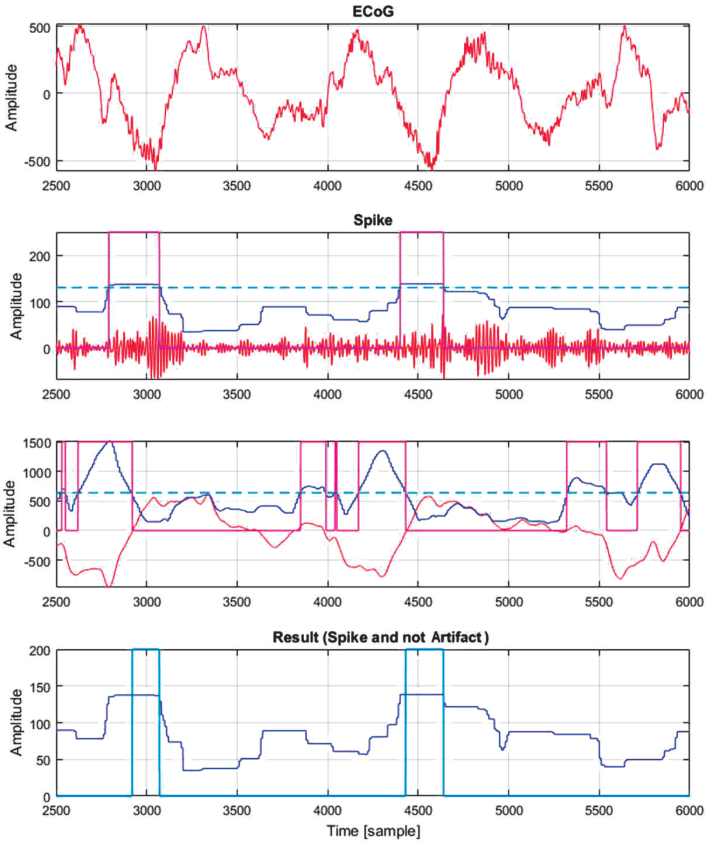

Fig. 8. Average spike/poly-spike amplitudes determined for all the ECoG signals in the intermediate stages of the analysis.

Unfortunately, such an analysis did not enable the removal of all artefacts. Additional methods were used to eliminate other artefacts, such as artefacts at high frequencies that usually occur on all electrodes, artefacts of "floating electrodes," and high-frequency artefacts. It was found experimentally that in a selected signal segment the number of spikes should not exceed a threshold of $P_k = 60\%$ and the number of spikes on a selected electrode should not be greater than $P_n = 50\%$. The electrodes for which these thresholds were exceeded were not included in the final result.

The correct performance of the algorithm depends on correctly set algorithm parameters. Theoretically, it is possible to select appropriate parameters for a single ECoG signal recording. This selection is possible only by iterative comparison of the result obtained with the algorithm with the result indicated by the neurologist. It requires a good understanding of the algorithm. It is a rather complicated and difficult process, especially as the results suggested by the neurologist should have be treated critically. Added to this is the interrelation of the key parameters. For example, if you change the settings for d parameter (window width), you would need to adjust the values of artefact detection threshold A_t and threshold for epilepsy discharges E_t. The problem of optimizing the threshold values is further complicated by the fact that each ECoG signal recording is different. This is mainly due to the layout of the electrode grid–individual for a

patient, as well as the amplitudes of the measured signals, including artefacts and discharges associated with epilepsy. Therefore, the only reasonable solution is to select the key parameters of the algorithm in an adaptive way, for a specific ECoG registration. Consequently, the manual selection of optimum parameters for all ECoG signals recording is almost impossible.

Either way, the proper setting of the key parameters of the algorithm can only be made by using a combination of medical knowledge and the knowledge about the algorithm operation. During the creation of the algorithm, the neurologist's behaviour during his manual analysis of ECoG signals was duplicated. Particular attention was paid to the mathematical description of all stages of the neurologist's work. It was a difficult process, because the neurologist performed part of the analysis basing on his intuition. It was difficult to define and describe his behaviour analytically. It has been observed that certain parameters can be invariable (very similar to each other) for all ECoG signal recordings. Based on the observations of the neurologist's work and the iterative execution of the algorithm, some constant parameters were chosen:

- low-pass $\boldsymbol{D}$ and band-pass $\boldsymbol{P}$ filters' parameters,
- a width of the time window expressed in the number of samples – d,
- a threshold for artefacts' elimination in rows – P_k, and
- a threshold for artefacts' elimination in columns – P_n.

Still, the problem of correct selection of other parameters remained unsolved:

- a threshold for detection of artefacts – A_t, and
- a threshold for detection of epileptic discharges – E_t.

Parameters of filters were determined on the basis of observations of the neurologist's work and the performed experiments. It was required that the filter bandwidth responsible for isolating spikes and poly-spikes was as narrow as possible, and a filter response had the greatest amplitude, against the background of other brain activity. Examples of ECoG signals and signals after the application of various band-pass filters are shown in Fig. 9. The spikes can be observed around values 750, 1,200, and 1,300. The greatest values of spike amplitudes, against the background of other activity, can be observed for the 12–20 Hz band-pass filter. It was decided to use a Butterworth filter of 4th order.

A similar analysis was performed for low frequencies associated with the "floating electrode" artefacts. In this case, it was decided to use a 2nd-order Butterworth low-pass filter with an upper limit of 3 Hz. Similar filters were used by the neurologists for the manual isolation of artefacts and spikes/poly-spikes during their analyses. During the program testing, we changed filter bandwidth values several times by several Hz for both spikes and artefacts. No significant changes in the algorithm performance were observed.

A width of the time window was adjusted on the basis of the observed variation of the ECoG signal. During the experiments, this width was changed from 0.5 s to 2 s. We adopted the value of 1 s as the window width. At first, the window was moved by one sample at a time. Such an approach was computationally expensive. Therefore, it was assumed to move the window every 10 samples. This resulted in a significant acceleration of the program.

Within the windowed signal, the amplitudes of spikes/poly-spikes or artefacts were determined. During the experiments, several methods were used to determine the energy level of the signal in a 1-s time window. We tested the following parameters:

- the maximum amplitude of samples,
- the minimum amplitude of samples,
- the average value of sample amplitudes,
- variance of sample amplitudes,
- standard deviation of sample amplitudes, and
- the peak-to-peak amplitude value.

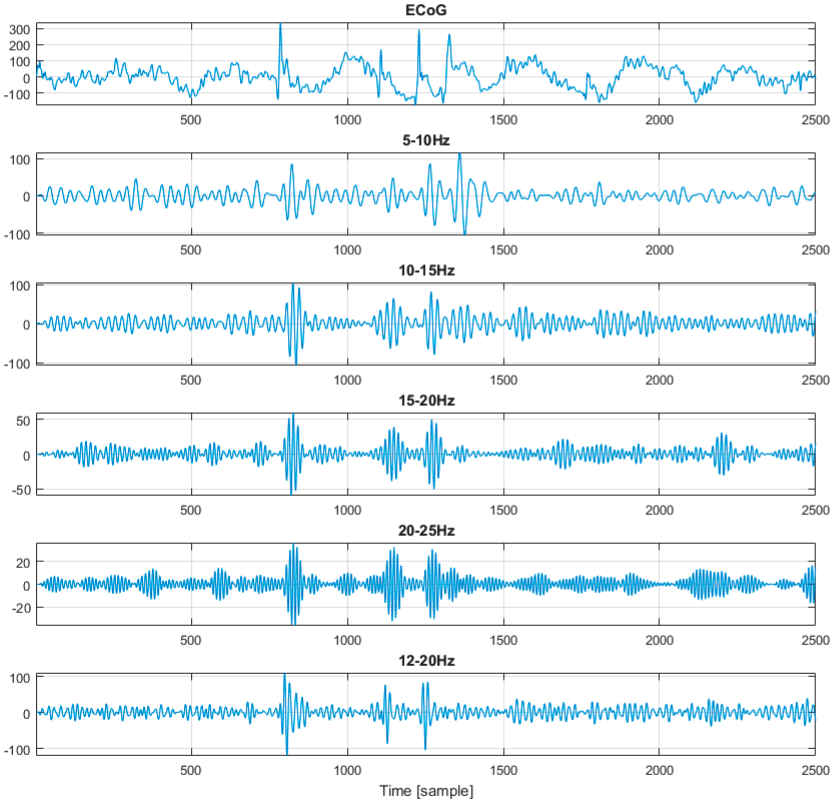

Fig. 9. ECoG signals and signals after the application of the band-pass filters.

There was no significant impact of the calculated energy content on the final result of analysis. Thus, we decided to use the peak-to-peak amplitude of the samples in the window.

The threshold values for the elimination of rows P_k and columns P_n were determined as a result of the observation of the neurologist's work. The P_k value was set to 60%, and the P_n threshold for the number of spikes on a selected electrode was set to 50%.

As already mentioned, the selection of A_t – the detection threshold for artefacts and E_t – the epilepsy discharge threshold parameter values is crucial for the correct operation of the algorithm. In addition, their selection is highly individualized and determined by the overall level of ECoG signals and the relative amplitude of artefacts and epileptic discharges–for each recording. A wrong choice of thresholds will most likely generate poor diagnostic results and, as a result, may lead to misdiagnosis. The threshold values can be selected based on detailed observations of spikes/poly-spikes and artefacts within the analysed signals. However, this type of selection takes a lot of time. In addition, visual evaluation of whether an ECoG signal fragment can be considered as an artefact or spike is problematic and requires a lot of experience.

Consequently, we decided to develop an automatic method for selecting the threshold values for the extraction of artefacts and spikes. This method is based on the quantitative analysis of the number of artefacts/spikes for a given threshold. A graph showing the percentages of artefacts and spikes after exceeding the established threshold values is presented in Fig. 10. On the basis

of the graph, there were selected the threshold values for which percentage changes could be read as:

– the largest percentage decrease in the number of spikes/poly-spikes, and
– the smallest decrease in the percentage of artefacts.

In this particular case, the threshold values are 131 for spikes/poly-spikes and 637 for artefacts. We considered several methods for automatic selection of these threshold values. As a result, we decided to use an MLP neural network.transfer of the collected data to a host controller.

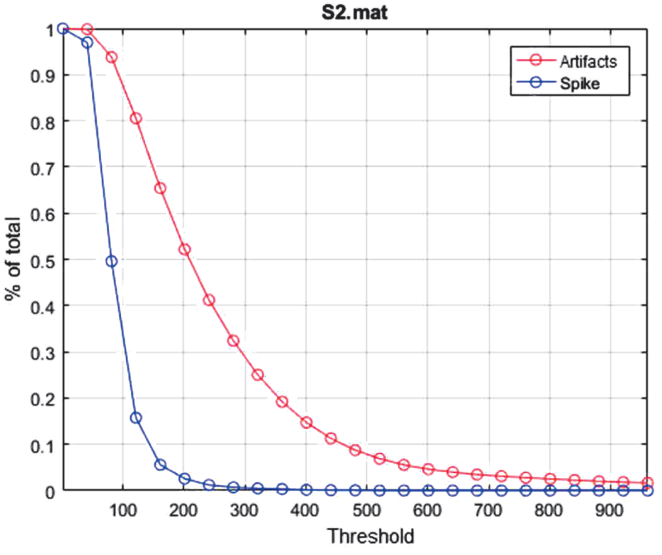

Fig. 10. A chart showing percentages of artefacts and spikes for different threshold values.

In order to teach the neural network, 20 artefact and spike threshold distributions (for data not included in the system test) were generated. Then, for each recording, the values of the largest drop for spikes and the greatest stabilization for artefacts were determined manually. Because the number of 20 cases was too small, a number of additional examples were artificially generated, adding Gaussian noise to curves. This enabled to change the curve slightly, and create new data. In this way, several hundred new learning examples were generated, and this made possible an effective MLP learning. The basic parameters of the created neural network are presented in Table 2.

Table 2. Basic parameters for the created neural network.

MLP parameter	Value/method
Number of inputs	25
Number of hidden layers	1
Number of neurons in the hidden layer	15
Number of outputs	1
Learning algorithm	Back propagation

The MLP network was tested for another 20 ECoG cases not included in the learning process. Only in two cases, the neural network incorrectly calculated the threshold values for determination artefact of artefacts or spikes. We hope that there is a chance to develop an even better and more effective method for selecting these thresholds.

As a result of the analysis of thirty-three cases of ECoG recordings, EZs were correctly identified for 29 registered sessions. In three cases, the neurologist found that the generated maps were not identical with the EZs identified during his analysis. Among these three cases, a probable cause of incorrect diagnosis were very large values of artefacts (two cases) that made the automatic selection of the artefact threshold for the MLP method not possible. However, after the manual selection of thresholds for artefacts and spikes, the results were found to be correct. For one case of incorrect diagnosis, very large discharges (in the beta band) were observed, similar to epileptic discharges.

6. Conclusion

Although many methods of ECoG analysis have been studied, the authors have not been able to find an algorithm for automatic EZ detection. In addition, no research was found in the literature dealing with a sufficiently large number of ECoG signals-recorded directly from the surface of the cerebral cortex. The presented results indicate that it is possible to identify EZ sites with an efficiency of 87.8%, thanks to the developed algorithm. As the effectiveness of correct location of the EZ is important, the algorithm can be a useful tool supporting the neurologist during the open-brain surgery.

Compliance with ethical standards

Ethical approval. All procedures performed in the studies involving human participants were in accordance with the ethical standards of the Medical University of Warsaw and with the 1964 Helsinki declaration and its later amendments or comparable ethical standards.

Informed consent. Informed consent was obtained from all individual participants.

Acknowledgements

This work was partly financed from the funds for the statutory activities of the Faculty of Electrical Engineering of the Warsaw University of Technology, under Dean's Grant in 2017.

References

[1] Messenheimer, J.A. (1991). Epilepsy: Frequency, causes and consequences. *J. Epilepsy*, 4(4), 246.

[2] Baumgartner, C., Lurger, S., Leutmezer F. (2001). Autonomic symptoms during epileptic seizures. *Epileptic Disord. Int. Epilepsy J. Videotape*, 3(3), 103–116.

[3] Guerrini, R., Scerrati, M., Rubboli, G., Esposito, V., Colicchio, G., Cossu, M., Marras, C.E.,Tassi, L., Tinuper P., Canevini, M.P., Quarato, P., Giordano, F., Granata, T., Villani, F., Giulioni, M., Scarpa, P., Barbieri, V., Bottini, G., Sole, A.D., Vatti, G., Spreafico, R., Russo, G.L. (2013). Overview of presurgical assessment and surgical treatment of epilepsy from the Italian League Against Epilepsy. *Epilepsia*, 54, 35–48.

[4] Tripathi, M., Garg, A., Gaikwad, S., Bal, C.S., Chitra, S., Prasad, K., Dash, H.H., Sharma, B.S., Chandra P.S. (2010). Intra-operative electrocorticography in lesional epilepsy. *Epilepsy Res.*, 89(1), 133–141.

[5] Hajek, M., Antonini, A., Leenders, K.L., Wieser, H.G. (1993). Mesiobasal versus lateral temporal lobe epilepsy Metabolic differences in the temporal lobe shown by interictal 18F-FDG positron emission tomography. *Neurology*, 43(1), 79–79.

[6] Dupont, S., Semah, F., Boon, P., Saint-Hilaire, J.M., Adam, C., Broglin, D., Baulac, M. (1999). Association of ipsilateral motor automatisms and contralateral dystonic posturing: a clinical feature differentiating medial from neocortical temporal lobe epilepsy. *Arch. Neurol.*, 56(8), 927–932.

[7] Blümcke, I., Thom, M., Aronica, E., Armstrong, D.D., Vinters H.V., Palmini, A., Jacques, T.S., Avanzini, G., Barkovich, A.J., Battaglia, G., Becker, A., Cepeda, C., Cendes, F., Colombo, N., Crino, P., Cross, J.H., Delalande, O., Dubeau, F., Duncan, J., Guerrini, R., Kahane, P., Mathern, G., Najm, I., Ozkara, C., Raybaud, C., Represa, A., Roper, S.N., Salamon, N., Schulze-Bonhage, A., Tassi, L., Vezzani, A., Spreafico, R. (2011). The clinicopathologic spectrum of focal cortical dysplasias: a consensus classification proposed by an ad hoc Task Force of the ILAE Diagnostic Methods Commission. *Epilepsia*, 52(1), 158–174.

[8] Bozek-Juzmicki, M., Colella, D., Jacyna, G.M. (1994). Feature-based epileptic seizure detection and prediction from ECoG recordings. *Proc. of IEEE-SP International Symposium on Time- Frequency and Time-Scale Analysis*, 564–567.

[9] Hill, N.J., Gupta, D., Brunner, P., Gunduz, A., Adamo, M.A., Ritaccio, A., Schalk, G. (2012). Recording human electrocorticographic (ECoG) signals for neuroscientific research and real-time functional cortical mapping. *J. Vis. Exp. JoVE*, (64).

[10] Gotman, J. (1999). Automatic detection of seizures and spikes. *J. Clin. Neurophysiol. Off. Publ. Am. Electroencephalogr. Soc.*, 16(2), 130–140.

[11] McGrogan N.S., Tarassenko, L. (1999). *Neural Network Detection of Epileptic Seizures in the Electroencephalogram*.

[12] Harner, R. (2009). Automatic EEG Spike Detection. *Clin. EEG Neurosci.*, 40(4), 262–270.

[13] Dümpelmann, M., Elger, C.E. (1998). Automatic detection of epileptiform spikes in the electrocorticogram: a comparison of two algorithms. *Seizure*, 7(2), 145–152.

[14] Wilson, S. B., Turner, C.A., Emerson, R.G., Scheuer, M.L. (1999). Spike detection II: automatic, perception-based detection and clustering. *Clinical Neurophysiology*, 110(3), 404–411.

[15] Webber, W.R., Litt, B., Wilson, K., Lesser R.P. (1994). Practical Detection of Epileptiform Discharges (EDs) in the EEG Using an Artificial Neural Network: A Comparison of Raw and Parameterized EEG Data. *PubMed Journals*, 91(3), 194–204.

[16] Fan, J., Shao, C., Ouyang, Y., Wang, J., Li, S., Wang, Z. (2006). Automatic Seizure Detection Based on Support Vector Machines with Genetic Algorithms. *Simulated Evolution and Learning*, 845–852.

[17] Exarchos, T.P., Tzallas, A.T., Fotiadis, D.I., Konitsiotis, S., Giannopoulos, S. (2006). EEG Transient Event Detection and Classification Using Association Rules. *IEEE Trans. Inf. Technol. Biomed.*, 10(3), 451–457.

[18] Srinivasan, V., Eswaran, C., Sriraam, N. (2005). Artificial Neural Network Based Epileptic Detection Using Time-Domain and Frequency-Domain Features *J. Med. Syst.*, 29(6), 647–660.

[19] Polat, K., Güneş, S. (2007). Classification of epileptiform EEG using a hybrid system based on decision tree classifier and fast Fourier transform. *Appl. Math. Comput.*, 187(2),1017–1026.

[20] Übeyli, E.D., Güler, İ. (1996). Features extracted by eigenvector methods for detecting variability of EEG signals. *Pattern Recognit. Lett.*, 28(5), 592–603.

[21] Iasemidis, L.D., Sackellares, J.C. (1996). REVIEW: Chaos Theory and Epilepsy. *The Neuroscientist*, 2(2), 118–126.

[22] Kannathal, N., Acharya, U.R., Lim, C.M., Sadasivan, P.K. (2005). Characterization of EEG – A comparative study. *Comput. Methods Programs Biomed.*, 80(1), 17–23.

[23] Lerner, D.E. (1996). Monitoring changing dynamics with correlation integrals: Case study of an epileptic seizure. *Phys. Nonlinear Phenom.*, 97(4), 563–576.

[24] Srinivasan, V., Eswaran, C., Sriraam, N. (2007). Approximate entropy-based epileptic EEG detection using artificial neural networks. *IEEE Trans. Inf. Technol. Biomed. Publ. IEEE Eng. Med. Biol. Soc.*, 11(3), 288–295.

[25] Osowski, S., Swiderski, B., Cichocki, A., Rysz, A. (2007). Epileptic seizure characterization by Lyapunov exponent of EEG signal. *COMPEL – Int. J. Comput. Math. Electr. Electron. Eng.*, 26(5), 1276–1287.

[26] Schwab, M., Schmidt, K., Witte, H., Abrams, R.M. (2000). Investigation of Nonlinear ECoG Changes during Spontaneous Sleep State Changes and Cortical Arousal in Fetal Sheep. *Cereb. Cortex*, 10(2), 142–148.